

₁ Study of neutrino-nucleus interaction at around 1 GeV using
₂ hollow cuboid lattice neutrino detectors, WAGASCI, muon
₃ range detectors and magnetized spectrometer, Baby MIND,
₄ at J-PARC neutrino monitor hall

₅ A. Bonnemaison, R. Cornat, L. Domine, O. Drapier, O. Ferreira, F. Gastaldi,
₆ M. Gonin, J. Imber, M. Licciardi, F. Magniette, T. Mueller, L. Vignoli, and O. Volcy

₇ *Ecole Polytechnique, IN2P3-CNRS, Laboratoire Leprince-Ringuet, Palaiseau,*
₈ *France*

₉ S. Cao and T. Kobayashi

₁₀ *High Energy Accelerator Research Organization (KEK), Tsukuba, Ibaraki, Japan*

₁₁ M. Khabibullin, A. Khotjantsev, A. Kostin, Y. Kudenko, A. Mefodiev, O. Mineev,
₁₂ S. Suvorov, and N. Yershov

₁₃ *Institute for Nuclear Research of the Russian Academy of Sciences, Moscow, Russia*

₁₄ B. Quilain

₁₅ *Kavli Institute for the Physics and Mathematics of the Universe (WPI), The*
₁₆ *University of Tokyo Institutes for Advanced Study, University of Tokyo, Kashiwa,*
₁₇ *Chiba, Japan*

₁₈ T. Hayashino, A. Hiramoto, A.K. Ichikawa, K. Nakamura, T. Nakaya, K Yasutome,
₁₉ and K. Yoshida

₂₀ *Kyoto University, Department of Physics, Kyoto, Japan*

₂₁ Y. Azuma, J. Harada, T. Inoue, K. Kin, N. Kukita, S. Tanaka, Y. Seiya,
₂₂ K. Wakamatsu, and K. Yamamoto

₂₃ *Osaka City University, Department of Physics, Osaka, Japan*

²⁴ A. Blondel, F. Cadoux, Y. Favere, E. Noah, L. Nicola, and S. Parsa

²⁵ *University of Geneva, Section de Physique, DPNC, Geneva, Switzerland*

²⁶ N. Chikuma, F. Hosomi, T. Koga, R. Tamura, and M. Yokoyama

²⁷ *University of Tokyo, Department of Physics, Tokyo, Japan*

²⁸ Y. Hayato

²⁹ *University of Tokyo, Institute for Cosmic Ray Research, Kamioka Observatory,
30 Kamioka, Japan*

³¹ Y. Asada, K. Matsushita, A. Minamino, K. Okamoto, and D. Yamaguchi

³² *Yokohama National University, Faculty of Engineering, Yokohama, Japan*

³³ December 14, 2017

34 Contents

35	1	Introduction	4
36	2	Experimental Setup	4
37	2.1	WAGASCI modules	6
38	2.1.1	Detector	6
39	2.1.2	Electronics	9
40	2.1.3	Water system	11
41	2.2	INGRID Proton module	11
42	2.3	Baby MIND	12
43	2.3.1	Magnet modules	12
44	2.3.2	Scintillator modules	13
45	2.3.3	Electronics	14
46	2.3.4	Pefromance check	16
47	2.4	Side muon range detector	16
48	3	Physics goals	18
49	3.1	Expected number of events	19
50	3.2	Pseudo-monochromatic beam by using different off-axis fluxes	19
51	3.3	Extraction of Cross sections	20
52	3.4	Subjects WAGASCI can contribute	21
53	4	Status of J-PARC T59 experiment	23
54	5	MC studies	26
55	5.1	Simulation setup	26
56	5.2	Event selection	26
57	6	Standalone WAGASCI-module performances	29
58	6.1	Reconstruction algorithm	32
59	6.1.1	Description	32
60	6.1.2	Performances	33
61	6.2	Background substraction: the water-out module	37
62	7	Schedule	40
63	8	Requests	40
64	8.1	Neutrino beam	40
65	8.2	Equipment request including power line	40

66 **1 Introduction**

67 The understanding of neutrino-nucleus interactions in the 1 GeV energy region is critical
68 for the success of accelerator-based neutrino oscillation experiments such as the T2K exper-
69 iment. Complicated multi-body effects of nuclei render this understanding difficult. The
70 T2K near detectors have been measuring these and significant progress has been achieved.
71 However, the understanding is still limited. One of the big factors preventing a complete
72 understanding is the non-monochromatic neutrino beam spectrum. Measurements with
73 distinct but partially overlapping beam spectra would be a great benefit in resolving the
74 contribution from different neutrino energies. We, the WAGASCI collaboration, proposes
75 to study the neutrino-nucleus interaction at the B2 floor of the neutrino monitor building,
76 where different neutrino spectra from the T2K off-axis near detector (ND280) can be ob-
77 tained due to the different off-axis position. Our experimental setup contains two hollow
78 cuboid lattice detectors as the neutrino interaction target (known as WAGASCI modules),
79 two side- and one downstream- muon range detectors(MRD's). We will have two types of
80 the WAGASCI modules, a water-in module and a water-out module. The water-in WA-
81 GASCI module has water the hollow cuboid lattice, and the water-out WAGASCI module
82 doesn't have water inside the lattice. The hollow cuboid lattice and side-MRD's allow a
83 measurement of wider-angle scattering than ND280. High water to scintillator material
84 ratio enables the measurement of the neutrino interaction with water, which is highly de-
85 sired for the T2K experiment because it's far detector, Super-Kamiokande, is composed of
86 water. The MRD's consist of plastic scintillators and iron plates. The downstream-MRD,
87 so called the Baby MIND detector, also works as a magnet and provides the charge iden-
88 tification capability as well as magnetic momentum measurement for high energy muons.
89 The charge identification is essentially important to select antineutrino events in the an-
90 tineutrino beam because contamination of the neutrino events is as high as 30%. Most of
91 the detectors have already been constructed. The WAGASCI modules have been commis-
92 sioned as the J-PARC T59 experiment and the Baby MIND detector was commissioned at
93 the CERN neutrino platform. Therefore, the collaboration will be ready to proceed to the
94 physics data taking for the T2K beam time in January 2019. We will provide the cross sec-
95 tions of the charged current neutrino and antineutrino interactions on water with slightly
96 higher neutrino energy than T2K ND280 with wide angler acceptance. When combined
97 with ND280 measurements, our measurement would greatly improve the understanding
98 of the neutrino interaction at around 1 GeV and contribute to reducing one of the most
99 significant uncertainties of the T2K experiment.

100 **2 Experimental Setup**

101 Figure 1 and 2 show a schematic view and a CAD drawing of the entire set of detectors.
102 Central neutrino target detectors consist of two WAGASCI modules and T2K INGRID
103 proton module. Inside the WAGASCI module, plastic scintillator bars are aligned as a

104 hollow cuboid lattice and spaces in the lattice are filled with water for a water-in WAGASCI
105 module. T2K INGRID proton module is a full active neutrino target detector which is
106 composed only with scintillator bars in its tracking region. The central detectors are
107 surrounded by two side- and one downstream- muon range detectors(MRD's) The MRD's
108 are used to select muon tracks from the charged-current (CC) interactions and to reject
109 short tracks caused by neutral particles that originate mainly from neutrino interactions in
110 material surrounding the central detector, like the walls of the detector hall, neutrons and
111 gammas, or neutral-current (NC) interactions. The muon momentum can be reconstructed
112 from its range inside the detector. The MRD's consist of plastic scintillators and iron plates.
113 The downstream-MRD, also known as the Baby MIND detector, additionally has a coil
114 wound around each of the iron plates so it may be magnetized. This provides the charge
115 selection capability.

116 For all detectors, scintillation light in the scintillator bar is collected and transported
117 to a photodetector with a wavelength shifting fiber (WLS fiber). The light is read out by
118 a photodetector, Multi-Pixel Photon Counter (MPPC), attached to one end of the WLS
119 fiber. The signal from the MPPC is read out by the dedicated electronics developed for
120 the test experiment to enable bunch separation in the beam spill. The readout electronics
121 are triggered using the beam-timing signal from MR to synchronize to the beam. The
122 beam-timing signal is branched from those for T2K, and will not effect T2K data taking.

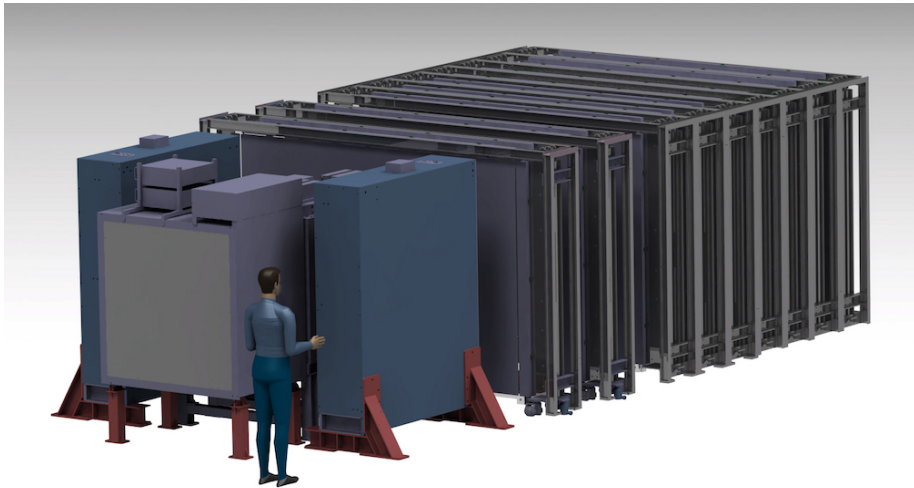


Figure 1: Schematic view of entire sets of detectors.

123 T2K adopted the off-axis beam method, in which the neutrino beam is intentionally
124 directed 2.5 degrees away from SK producing a narrow band ν_μ beam. The off-axis near
125 detector, ND280, is installed towards the SK direction in the B1 floor of the near detector

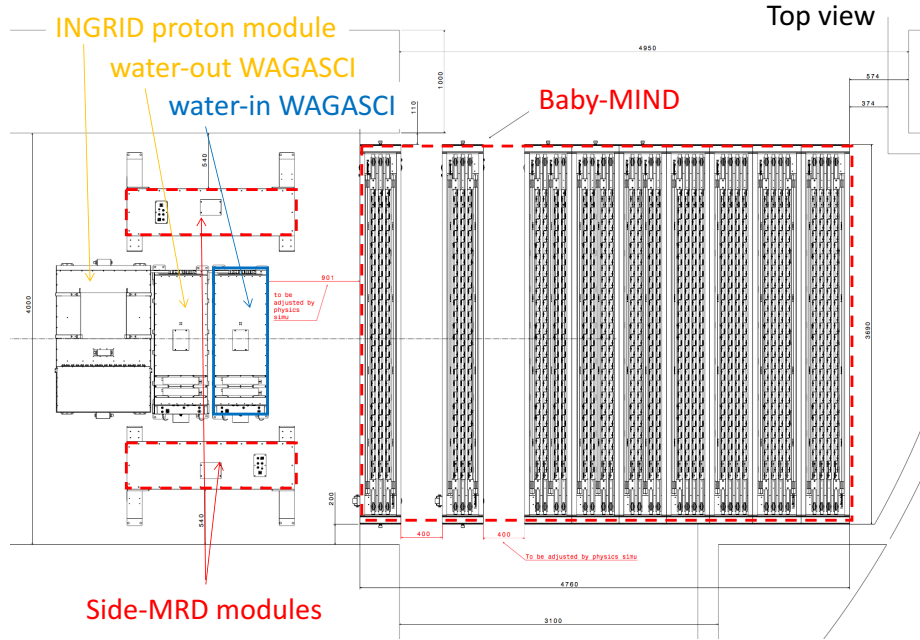


Figure 2: Top view of entire sets of detectors.

126 hall of the J-PARC neutrino beam-line. We propose to install our detector in the B2 floor
 127 of the near detector hall, where the off-axis angle of 1.5 degrees is slightly different to the
 128 2.5 degrees of ND280. The candidate detector position in the B2 floor is shown in Figure
 129 3. The expected neutrino energy spectrum at the candidate position is shown in Figure 4.

130 **2.1 WAGASCI modules**

131 **2.1.1 Detector**

132 The WAGASCI modules are mainly composed of 1280 plastic scintillator bars and a sur-
 133 rounding stainless steel tank as shown in Figure 5. The total number of channels in one
 134 WAGASCI module is 1280. The stainless steel tank is constructed by welding stainless
 135 steel plates, is sized as 460mm×1250mm×1250 mm, and weighs 0.5 tonne.

136 One WAGASCI module consists of 16 scintillator tracking planes, where each plane
 137 is an array of 80 scintillator bars fixed with ABS frames. The 40 bars, called parallel
 138 scintillators, are placed perpendicularly to the beam, and the other 40 bars, called lattice
 139 scintillators, are placed in parallel to the beam with hollow cuboid lattice in the tracking
 140 plane as shown in Figure 5. Thanks to the hollow cuboid lattice of the scintillator bars,

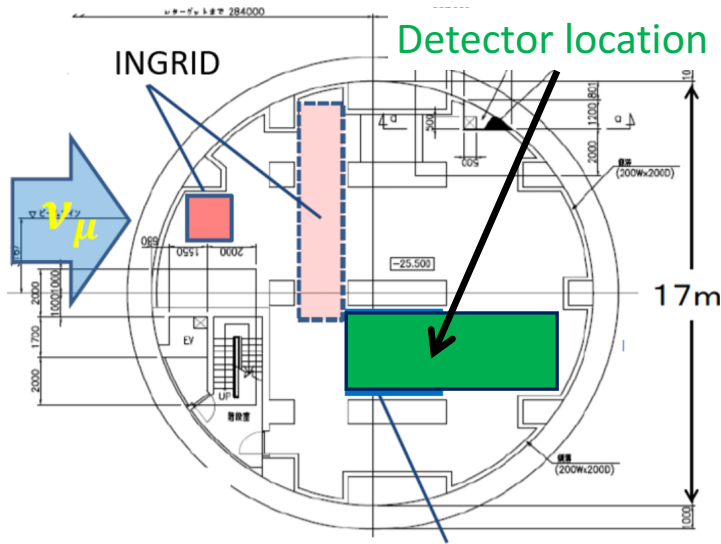


Figure 3: Candidate detector position on the B2 floor of the near detector hall.

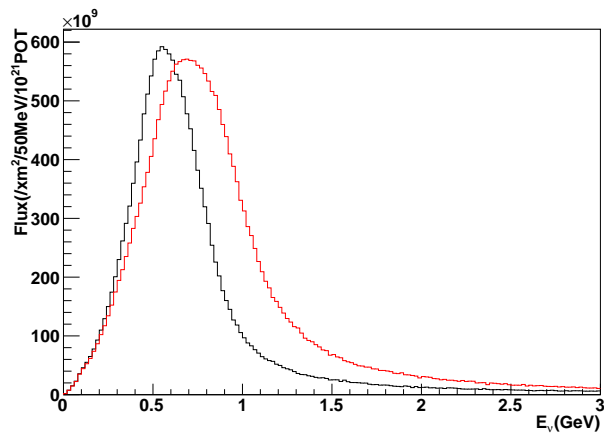


Figure 4: Neutrino energy spectrum at the candidate detector position (red, off-axis 1.5 degree). The spectrum at the ND280 site (black, off-axis 2.5 degree) is also shown.

141 the WAGASCI module has 4π angular acceptance for charged particles.

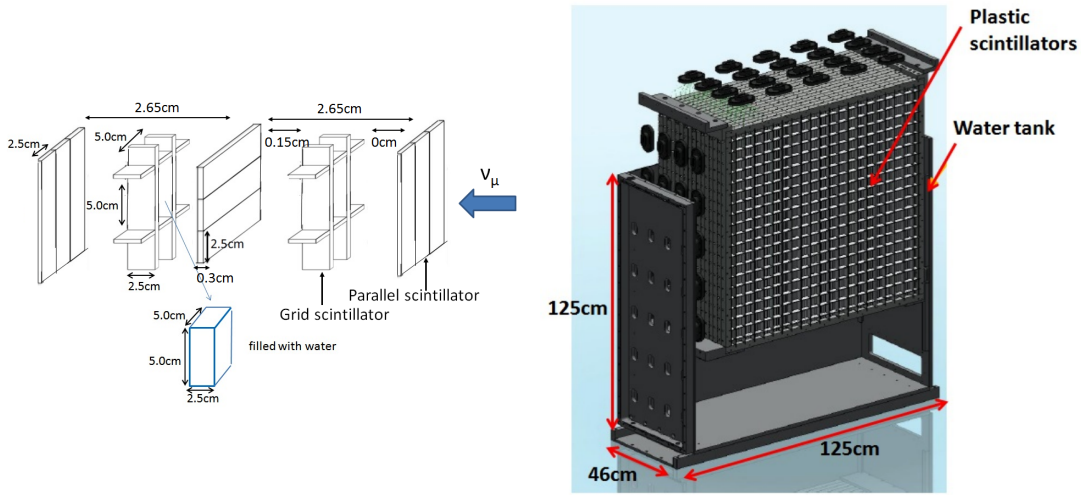


Figure 5: Schematic views of hollow cuboid lattice of plastic scintillator bars (left) and WAGASCI module (right).

142 Thin plastic scintillator bars produced at Fermilab by extrusion method, mainly consists
143 of polystyrene and are surrounded by thin reflector including TiO^2 (3 mm in thickness)
144 are used for the WAGASCI modules to reduce the mass ratio of scintillator bars to water,
145 because neutrino interactions in the scintillator bars are a background for the cross section
146 measurements on H_2O . Each scintillator bar is sized as 1020mm \times 25mm \times 3 mm including
147 the reflector part, and half of all the scintillator bars have 50-mm-interval slits to form the
148 hollow cuboid lattice (Figure 6).

149 We will have two types of the WAGASCI modules, a water-in module and a water-out
150 module. The water-in WAGASCI module has water in spaces of the hollow cuboid lattice.
151 The total water mass serving as neutrino targets in the fiducial volume of the module is
152 188 kg, and the mass ratio of scintillator bars to water is 80 %. The water-out WAGASCI
153 module doesn't have water inside the detector. The total CH mass serving as neutrino
154 target in the fiducial volume of the module is 47 kg, and the mass fraction of scintillator
155 bars is 100 %.

156 Scintillation light is collected by wave length shifting fibers, Y-11 (non-S type with a
157 diameter of 1.0 mm produced by Kuraray. A fiber is glued by optical cement in a groove
158 on surface of a scintillator bar. 32 fibers are gathered together by a fiber bundle at edge
159 of the module, and lead scintillation light to a 32-channel arrayed MPPC. Since crosstalk
160 of light yield due to reflection on the inner surface of each cell has been observed, all the
161 scintillator bars are painted black by aqueous color spray. It is confirmed by measurements
162 with cosmic rays that black painting on the surface of the scintillator bars suppresses this

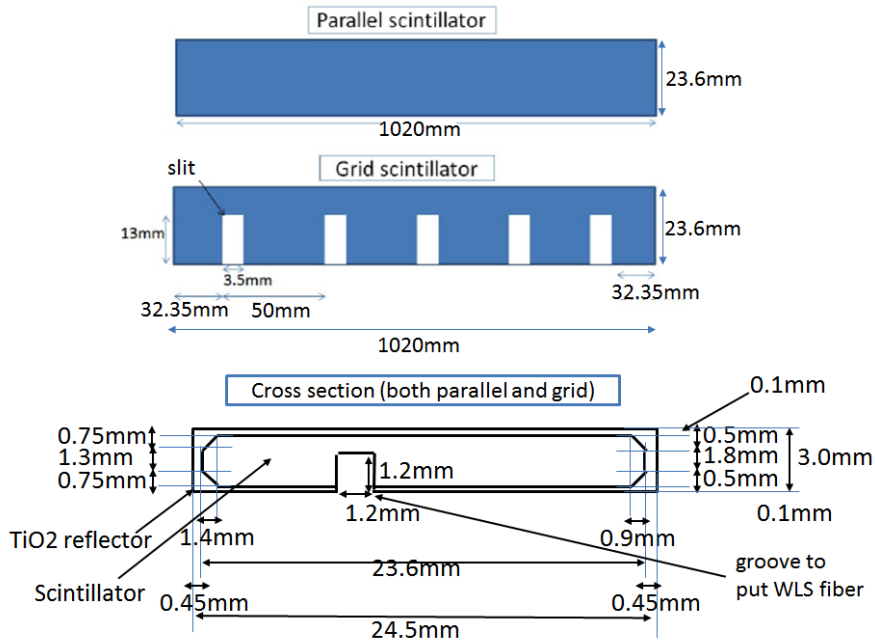


Figure 6: Geometry of scintillators used for WAGASCI modules.

163 crosstalk so that no significant crosstalk effect is observed within uncertainty.

164 32-channel arrayed MPPCs, as shown in the Figure 7, are used for the modules. The
 165 surface of the fiber bundle is polished and directly attached onto the 32-channel arrayed
 166 MPPCs. The positions of 32 fibers on the bundle are aligned to fit the channels of MPPCs.
 167 The MPPC is a product of Hamamatsu Photonics, S13660(ES1), with suppressed noise
 168 rate of ~ 6 kHz per channel at 0.5 p.e. threshold. For each MPPC channel, 716 pixels of
 169 APD are aligned in a shape of circle.

170 **2.1.2 Electronics**

171 As front-end electronics of this detector, a Silicon PM Integrated Read-Out Chip (SPIROC)
 172 [13] is adopted. SPIROC is a 36-channel auto-triggered front-end ASIC, and is produced
 173 by OMEGA/ IN2P3. It not only contains an analog signal processing part such as amplification
 174 and shaping of the waveform, but contains a digital signal processing parts such as
 175 auto-trigger and timing measurement. Charge of MPPC signal is sampled by track-and-
 176 hold circuit. A Front-end electronics board, Active Sensor Unit (ASU), has been developed
 177 with the SPIROC2D chip, which is the latest version of SPIROC. Each readout board is
 178 designed to control a 32-channel arrayed MPPC, and 40 of the ASU boards are aligned on
 179 the module surface. The data acquisition system used for this detector, including back-end

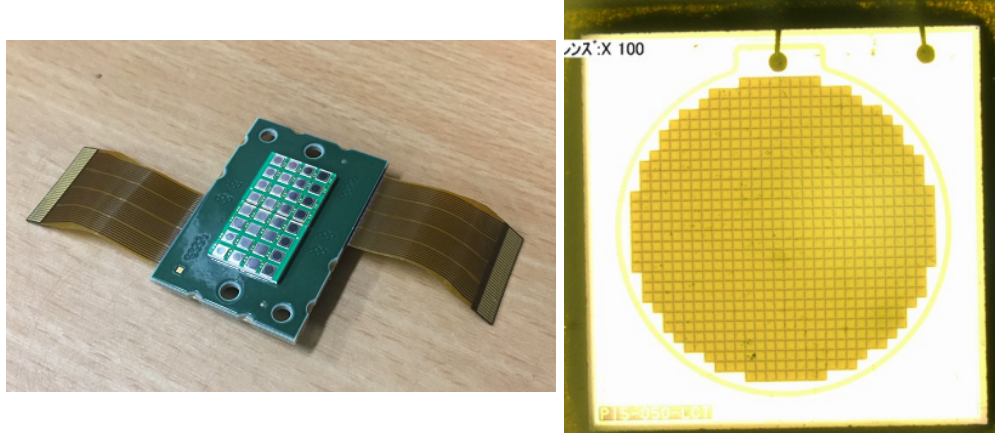


Figure 7: 32-channel arrayed MPPC (left) and an enlarged view of one MPPC channel (right).

boards, has been developed for prototypes of ultra-granular calorimeters for the International Linear Collider (ILC) [6], and independent of the T2K DAQ system. To synchronize the DAQ system to J- PARC neutrino beam, pre-beam trigger and beam trigger are sent to the clock control card. The beam trigger signals are converted from optical signals to NIM signals at NIM module on the B2 floor. In addition, the information of spill number are delivered with 16-bit ECL level signals, and converted to an Ethernet frame by an FPGA evaluation board to be directly sent to the DAQ PC. The electronics readout scheme is shown in Figure 8.

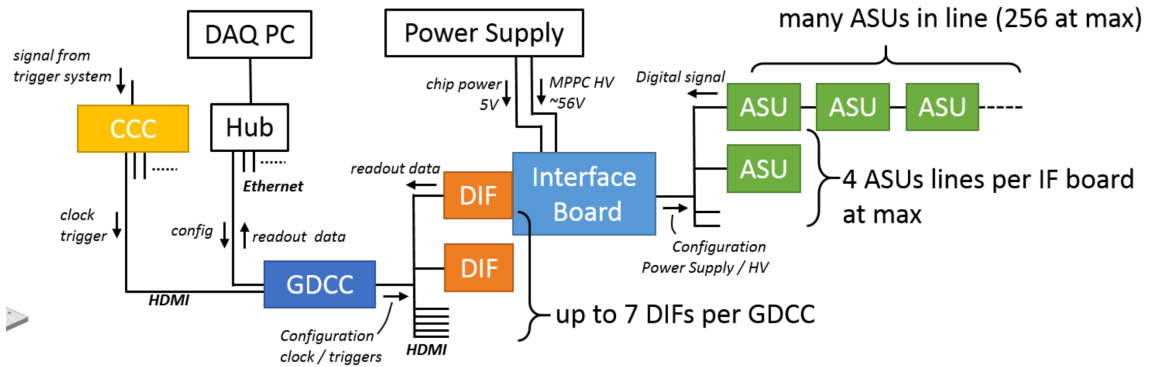


Figure 8: WAGASCI electronics readout scheme.

188 **2.1.3 Water system**

189 Pure water is filled to the water tank of the water-in WAGASCI module as follows. First,
190 the water storage tank located at the B2 floor of the NM pit is filled with water delivered
191 from a water tap on the ground level through a long hose. Second, the water is pumped
192 to the other water storage tank though a water filler to produce pure water. Third, a
193 compound preservative called Germall plus, which is the same preservative used in one of
194 the sub-detectors of T2K ND280, FGD2, is put into the water to keep water from being
195 bad. Then, the water is poured to the water-in WAGASCI module, and it is kept in the
196 module during the neutrino beam operation and not to be circulated.

197 **2.2 INGRID Proton module**

198 INGRID Proton module is a neutrino detector of the T2K experiment. It is a fully-active
199 tracking detector which consists of only scintillator strips. The purpose of this Proton
200 Module is to separate the neutrino interaction types by detecting the protons and pions
201 together with the muons from the neutrino interactions, and to measure the neutrino cross
202 section for each interaction type. It consists of 36 tracking planes surrounded by veto
203 planes (Figure 9), where each tracking plane is an array of two types of scintillator strips.
204 The 16 strips in the inner region have dimensions of $25\text{mm} \times 13\text{mm} \times 1200\text{mm}$, while the 16
205 strips in the outer region have dimensions of $50\text{mm} \times 10\text{mm} \times 1200\text{mm}$, making a plane of
206 $1200\text{mm} \times 1200\text{mm}$ in the horizontal and vertical directions. The former is the scintillator
207 produced for the K2K SciBar detector [4] and the latter was produced for INGRID. The
208 tracking planes are placed perpendicular to the beam axis at 23mm intervals. Since the
209 strips are aligned in one direction, each tracking plane is sensitive to either the horizontal or
210 vertical position of the tracks. The tracking planes are therefore placed alternating in the
211 horizontal and vertical directions so that three-dimensional tracks can be reconstructed.
212 The tracking planes also serve as the neutrino interaction target. As with the WAGASCI
213 modules, scintillation light is read out by a WLS fiber and MPPC.

214 It was installed on the neutrino beam axis on the SS floor of the T2K near detector hall
215 in 2010, and had been used for neutrino cross section measurements. In August 2017, it
216 was moved to the B2 floor of the T2K near detector hall by J-PARC T59 after getting the
217 approval from T2K to use them. J-PARC T59 is performing a neutrino beam measurement
218 using the detector from October 2017, and the measurement will continue until May 2018
219 as we will discuss in Sec. 4.

220 We will operate the INGRID Proton module using the T2K near detector electronics/
221 DAQ system in the same way as J-PARC T59. A proposal to use the module and its
222 electronics for our project will be submitted to the T2K collaboration.

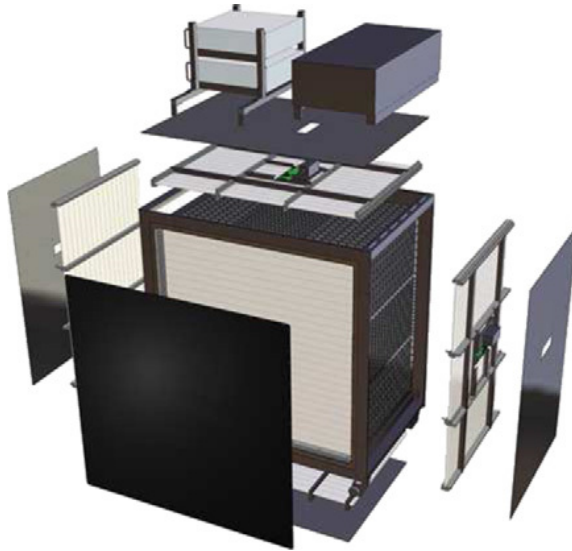


Figure 9: Schematic view of INGRID Proton module.

2.3 Baby MIND

The Baby MIND is the downstream Muon Range Detector. It also works as a magnet and provides the charge identification capability as well as magnetic momentum measurement for high energy muons.

The Baby MIND collaboration ¹ submitted a proposal to the SPSC at CERN, SPSC-P-353. The project was approved by the CERN research board as Neutrino Platform project NP05 and constructed. The detector consists of 33 magnet modules, each 3500 mm × 2000 mm × 50 mm (30 mm steel) with a mass of approximately 2 tonnes. Of these magnet modules, 18 are instrumented with plastic scintillator modules.

2.3.1 Magnet modules

Traditional layouts for magnetized iron neutrino detectors (e.g. MINOS) tend to be monolithic blocks with a unique pitch between consecutive steel segments and large conductor coils threaded around the whole magnet volume. The Baby MIND detector, like traditional designs, is built from sheets of iron interleaved with scintillator detector modules. However Baby MIND is novel in that the iron segments are all individually magnetized as shown in Figure 10, allowing for far greater flexibility in the setting of the pitch between segments, and in the allowable geometries that these detectors can take.

¹Contact person: E. Noah, Spokesperson: A. Blondel, Deputy spokesperson: Y. Kudenko

240 The key design outcome is a highly optimized magnetic field map. A double-slit con-
 241 figuration for coil winding was adopted to increase the area over which the magnetic flux
 242 lines are homogeneous in B_x across the central tracking region. Simulations show the
 243 magnet field map to be very uniform over this central tracking region covering an area of
 244 $2800 \times 2000 \text{ mm}^2$, Figure 11. The B_x component dominates in this region, with negligible
 245 B_y and B_z . This was confirmed by measuring the field with 9 pick-up coils wound around
 246 the first module. Subsequent modules were equipped with one pick-up coil. Test results
 247 on the 33 modules show all achieve the required field of 1.5 T for a current of 140 A, with
 248 a total power consumption of 11.5 kW. The polarity of the field map shown in Figure 11
 (middle) can be reversed by changing the power supply configuration.

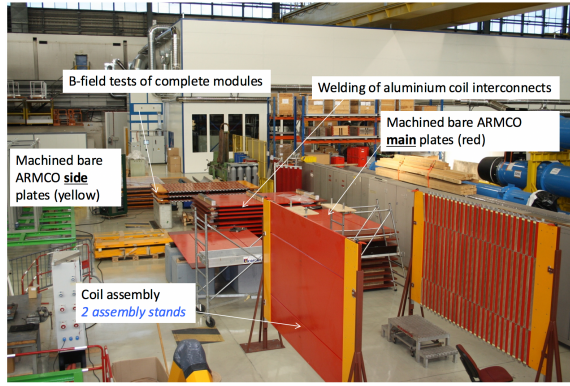


Figure 10: Magnet assembly zone at CERN.

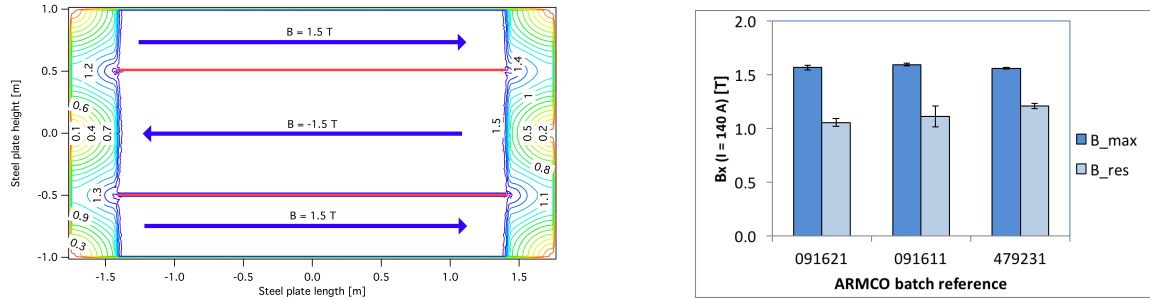


Figure 11: Left) Magnetic field map with a coil along 2800 mm of the length of the plate.
 Right) Measured B field for 33 modules.

249

250 2.3.2 Scintillator modules

251 Each of the 18 scintillator modules is constructed from 2 planes of horizontal counters (95
 252 counters in total) and 2 planes of vertical counters (16 counters in total) [3], arranged

253 with an overlap between planes to achieve close to 100% hit efficiency for minimum ionizing
254 muons. The arrangement of planes within a module is vertical-horizontal-horizontal-
255 vertical. This arrangement was the result of an assembly approach whereby each plane
256 was built from 2 half-planes, with each half plane consisting of a horizontal plane and a
257 vertical plane. The scintillator bars are held in place using structural ladders that align
258 and maintain the counters, Figure 12. No glue is used in the process, so counters can be
259 replaced. Aluminum sheets front and back provide light tightness.



Figure 12: Scintillator modules assembly. Left) top of front half-module showing vertical counters, and the spacer-ladders that set the pitch between horizontal counters and hold them in place. Middle) rear half-module showing horizontal counters on their ladders. Right) Assembled rear half-module, the front half-module can be seen in the background.

260 The plastic scintillator counters were made from 220 mm-wide slabs, consisting of
261 extruded polystyrene doped with 1.5% paraterphenyl (PTP) and 0.01% POPOP. They were
262 cut to size then covered with a 30-100 μm thick diffuse reflector resulting from etching of the
263 surface with a chemical agent [10, 11]. The horizontal counter size is $2880 \times 31 \times 7.5 \text{ mm}^3$,
264 with one groove along the length of the bar in which sits a wavelength shifting fiber from
265 Kuraray. The vertical counter size is $1950 \times 210 \times 7.5 \text{ mm}^3$, with one U-shaped groove
266 along the bar. On each counter, two custom connectors house silicon photomultipliers,
267 MPPC type S12571-025C from Hamamatsu, either side of the horizontal counter, and
268 both connectors at the top for the vertical counter. This geometrical configuration for
269 vertical counters was chosen for ease of connectivity to the electronics, and maintenance
270 operations.

271 A total of 1744 horizontal counters and 315 vertical counters (including spares) were
272 produced at the Uniplast company (Vladimir, Russia).

273 2.3.3 Electronics

274 The Baby MIND electronic readout scheme includes several custom-designed boards [12].
275 The revised version is shown in Figure 13. At the heart of the system is the electronics
276 Front End Board (FEB), developed by the University of Geneva. The readout system
277 includes two ancillary boards, the Backplane, and the Master Clock Board (MCB) whose
278 development has been managed by INRNE (Bulgarian Academy of Sciences) collaborators.

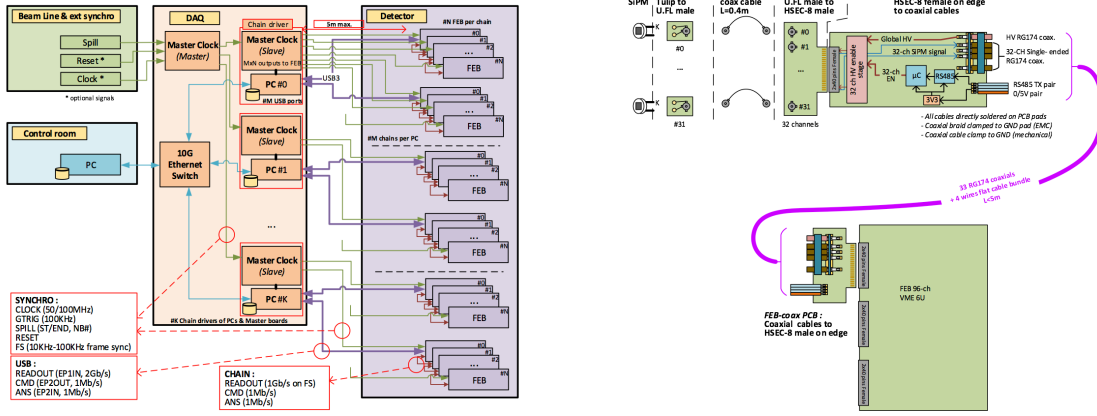


Figure 13: Left) Baby MIND electronics readout scheme. Right) SiPM-to-FEB connectivity.

279 The FEBv2 hosts 3 CITIROC chips that can each read in signals from 32 SiPMs [7].
280 Each signal input is processed by a high gain (HG), and a separate low gain (LG), signal
281 path. The outputs from the slow shapers can be sampled using one of two modes: a
282 mode with an externally applied delay, and a peak detector mode. A faster shaper can be
283 switched to either HG or LG paths, followed by discriminators with adjustable thresholds
284 providing 32 individual trigger outputs and one OR32 trigger output. An Altera ARIA5
285 FPGA on the FEBv2 samples these trigger outputs at 400 MHz, recording rising and falling
286 times for the individual triggers and assigning time stamps to these. Time-over-threshold,
287 the difference between falling and rising times, gives some measure of signal amplitude.
288 This is used in addition to charge information and proves useful if there is more than
289 one hit per bar within the $\sim 9 \mu\text{s}$ deadtime due to the readout of the multiplexed charge
290 output. The ARIA5 also manages the digitization of the sampled CITIROC multiplexed
291 HG and LG outputs via a 12-bit 8-ch ADC.

292 The internal 400 MHz clock on the FEBv2 can be synchronized to a common 100 MHz
293 clock. The synchronization subsystem combines input signals from the beam line into
294 a digital synchronization signal (SYNC) and produces a common detector clock (CLK)
295 which can eventually be synchronised to an external experiment clock. Both SYNC and
296 CLK signals are distributed to the FEBs. Tests show the FEB-to-FEB CLK(SYNC) delay
297 difference to be 50 ps (70 ps). Signals from the beam line at WAGASCI include two
298 separate timing signals, arriving 100 ms and 30 μs before the neutrino beam at the near
299 detectors. The spill number is available as a 16-bit signal.

300 **2.3.4 Pefromance check**

301 All counters were measured at INR Moscow with a cosmic ray setup using the same type
 302 S12571-025C MPPCs and a CAEN DT5742 digitizer. The average light yield (sum from
 303 both ends) was measured to be 37.5 photo-electrons (p.e.) per minimum ionizing particle
 304 (MIP) and 65 p.e./MIP for vertical and horizontal counters, respectively. After shipment
 305 to CERN, all counters were individually re-tested with an LED [?]. 0.1% of counters
 306 failed the LED tests and were therefore not used during the assembly of modules. The
 307 assembly of modules was completed in June 2017, and it was then tested in June and July
 308 2017 at the Proton Synchrotron experimental hall at CERN with a mixed particle beam
 309 comprising mostly muons whose momenta could be selected between 0.5 and 5 GeV/c. An
 event display from the summer 2017 tests is shown in Figure 14.

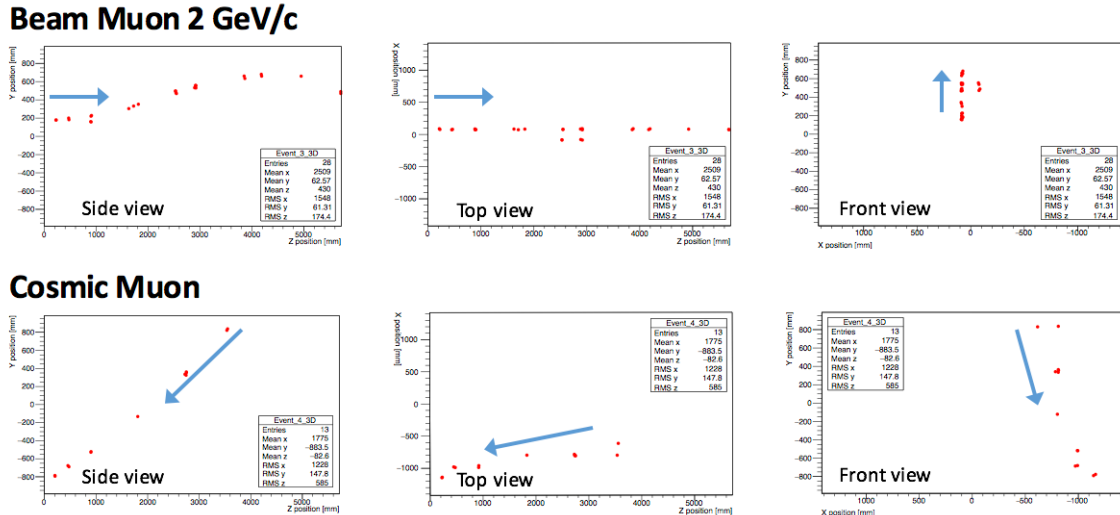


Figure 14: Comparison of a beam muon and cosmic muon in the three different geometrical projections of the detector. The beam impinges on the detector from the left. The arrows indicate the direction of travel of these muons. The direction of the cosmic muon is inferred from timing information.

310

311 **2.4 Side muon range detector**

312 Two Side-MRD modules for tracking secondary particles from neutrino interactions will be
 313 installed in 2018. Each Side-MRD module is composed of 11 steel plates and 80 scintillator
 314 slabs. The slabs are arranged as 10 layers installed in the 13 mm gaps between the 30 mm
 315 thick plates. Each steel plate size is 30 mm \times 1610 mm \times 1800 mm. Total module size is
 316 2236 mm \times 1630 mm \times 975 mm as shown in Figure 15 (left), weight is \sim 8.5 tonne.

317 Scintillator bars were manufactured by Uniplast company in Vladimir, Russia. Polystyrene
 318 based scintillators were extruded with thickness of 7 mm, then cut to the size of $7 \times 200 \times$
 319 1800 mm^3 . Dopant composition is 1.5% PTP and 0.01% POPOP. Scintillator surface was
 320 etched by a chemical agent to form a white diffuse layer with excellent reflective perfor-
 321 mance. Ideal contact between the scintillator and the reflector raises the light yield up
 322 to 50% comparing to an uncovered scintillator. A sinusoidal groove was milled along the
 323 scintillator to provide uniform light collection over the whole scintillator surface. WLS Y11
 324 Kuraray fiber of 1 mm diameter was glued with an optical cement EJ-500 in the S-shape
 325 groove as shown in Figure 15(right). A minimum bending radius of 30 mm was used to
 326 ensure the the Kuraray S-type fibers remained within specification. Both ends of the fiber
 327 were glued into optical connectors which were themselves attached to the scintillator and
 328 provide an interface to SiPMs, Hamamatsu MPPC S13081-050CS(X1).

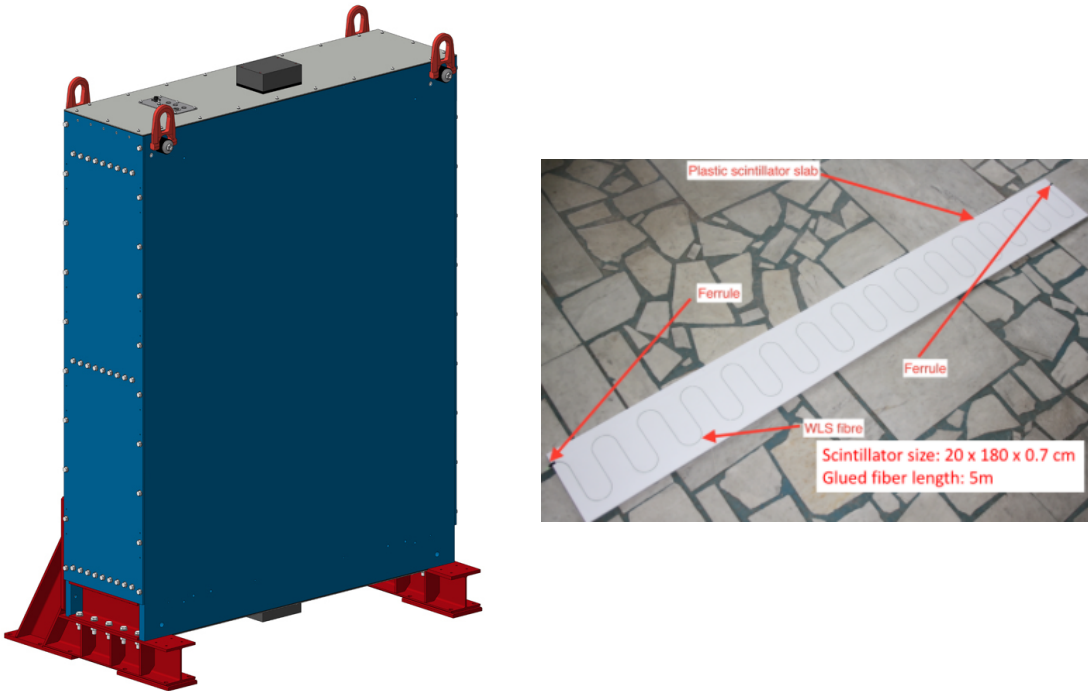


Figure 15: Left :Side-MRD module. Right: Scintillator bar of the Side-MRD modules.

329 Scintillators for the Side-MRD modules were assembled at INR in Russia, and shipped
 330 to Japan in July 2017. The light yield for each scintillator was measured with cosmic
 331 rays at INR and at YNU in Japan after delivery. LY_1 and LY_2 are light yields measured
 332 at both ends of the counter. The light yield asymmetry between the ends calculated as

333 $100\% \times \frac{LY_1 - LY_2}{LY_1 + LY_2}$. After tests at INR we selected 324 counters from measured 332 ones with
 334 the mean light yield of 45 p.e./MIP ($LY_1 + LY_2$) and the asymmetry value less than 10
 335 % . The measurements at YNU yielded the average total light yield of about 40 p.e./MIP
 336 which varies in range from 32 to 50 p.e./MIP (Figure 16 (left)). Only two counters showed
 337 relatively high asymmetry close to 25 % as shown in Figure 16 (right). Using the results of
 338 the quality assurance test we selected 320 scintillator counters for the Side-MRD modules.
 339

340 We also measured the time resolution for a combination of four counters piled one
 341 upon another. The average result for four counters is $\sigma_T = 1.04$ ns. The resolution of
 341 combination of 2, 3, 4 counters is measured to be 0.79 ns, 0.66 ns and 0.58 ns, respectively.
 341

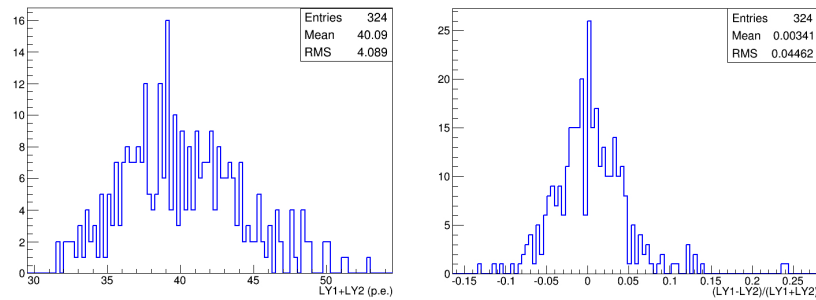


Figure 16: Total light yield distribution (left) and light yield assymetry (right) measured at YNU.

342
 343 Construction of the Side-MRD modules is scheduled from November 2017 at Yokohama
 344 National University. They will then be transported to J-PARC for installation on the B2
 345 floor of the T2K near detector hall.
 346

346 Same electronics as the WAGASCI modules (see Sec. 2.1.2) are used for the Side-MRD
 347 modules.
 347

3 Physics goals

348 We will measure the differential cross section for the charged-current (CC) interaction on
 349 H_2O and Hydrocarbon(CH)). The water-scintillator mass ratio of the WAGASCI module
 350 is as high as 4:1 and the high purity measurement of the cross section on H_2O is possible.
 351 One experimental option is to remove water from one of the two WAGASCI modules. The
 352 water-out WAGASCI module will allow to measure pure-CH target interactions with very
 353 low momentum-threshold for protons. This will also allow this CH interaction background
 354 to be subtracted from the water-in target measurement. Another option is to add the T2K
 355 proton module which is fully made of plastic scintillators. It will allow the high statistics
 356

357 comparison of cross section between H₂O and CH and also comparison with the ND280
358 measurement. The actual configuration will be optimized with detailed MC simulation by
359 2018 Summer.

360 Our setup allows the measurements of inclusive and also exclusive channels such as 1μ ,
361 $1\mu 1p$, $1\mu 1\pi^\pm np$ samples, the first two of which are mainly caused by the quasi-elastic and
362 2p2h interaction and the latter is mainly caused by resonant or coherent pion production
363 and deep elastic scattering. In general, an accelerator produced neutrino beam spectrum is
364 wide and the energy reconstruction depends upon the neutrino interaction model. Therefore,
365 recent neutrino cross section measurements including those from T2K are given as
366 a flux-integrated cross section rather than cross sections as a function of the neutrino en-
367 ergy to avoid the model dependency. We can provide the flux-integrated cross section.
368 In addition, by combining our measurements with those from ND280, model-independent
369 extraction of the cross section for narrow energy spread becomes possible. This method
370 was demonstrated in [1] and also proposed by E61 (NUPRISM) experiment.

371 **3.1 Expected number of events**

372 Expected number of CC neutrino events remaining after the event selections was evaluated
373 with simulation. Detailes are described in Sec. 5. In neutrino-mode, 5,400, 1,100 and 3,800
374 events are expected for the water-in WAGASCI module, the water-out WAGASCI module
375 and the INGRID proton module with 5×10^{20} POT. Among 5,400 events for the water-in
376 WAGASCI module, 78 % are interactions on H₂O. In the antineutrino-mode, 2,240, 400
377 and 1,500 CC antineutrino events are expected for the water-in WAGASCI module, the
378 water-out WAGASCI module and the INGRID proton module with 5×10^{20} POT. Amongh
379 2,240, 74 % are interactions on H₂O. The wrong-sign interactions in antineutrino-mode is
380 561 events, but will be removed with 90 % or higher efficiency by Baby MIND.

381 **3.2 Pseudo-monochromatic beam by using different off-axis fluxes**

382 The off-axis method gives narrower neutrino spectrum, and the peak energy is lower for
383 larger off-axis angle. There still remains a high energy tail mainly due to neutrinos from
384 Kaon decay. The off-axis angle of the WAGASCI location is 1.5 degrees as opposed to
385 2.5 degrees for ND280. Top two plots of Figure 17 show the energy spectra of fluxes and
386 neutrino interaction events at these two different location. Bottom two plots of Figure 17
387 show the energy spectra of fluxes and neutrino interaction events obtained by subtraction
388 of fluxes at ND280 and WAGASCI. We can effectively get two fluxes, from 0.2 GeV to
389 0.9 GeV and 0.6 GeV and 2 GeV and measure flux-integrated cross section for these two
390 fluxes. It should be noted that even though the statistical errors are drawn for each energy
391 bin for the bottom right plot of Fig. 17, measurement results will be given as an integration
392 across energies.

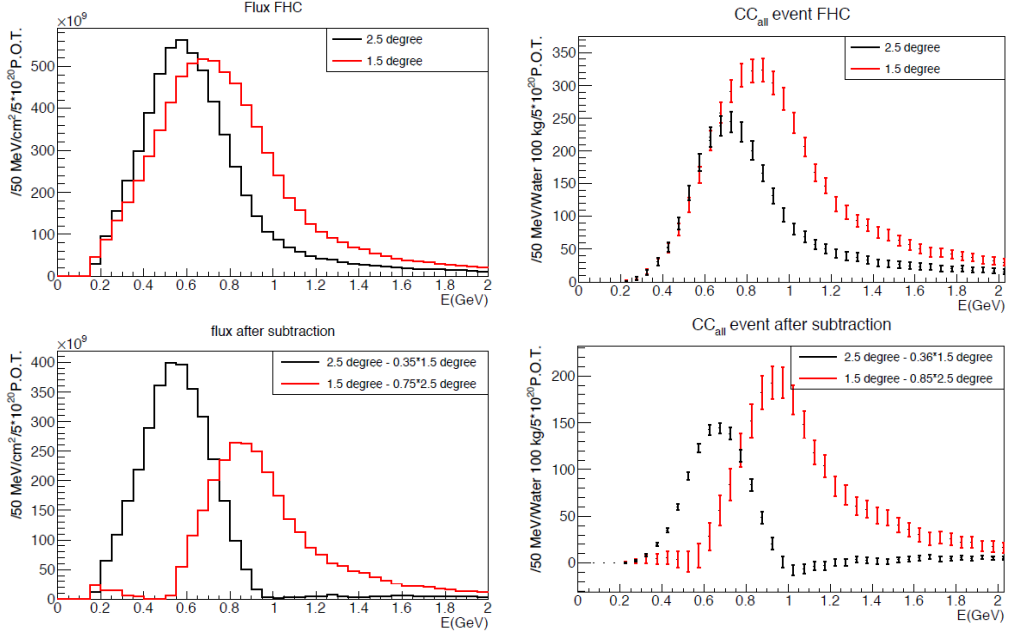


Figure 17: Energy spectra obtained by using different off-axis angle fluxes. Top two plots show the fluxes(left) and spectra of interaction events (right) for ND280 (off-axis 2.5 degree) and WAGASCI (off-axis 1.5 degree). Bottom two plots show the fluxes (left) and spectra of interaction events (right) obtained by subtraction of fluxes at ND280 and WAGASCI. The error bars represent the statistical error and those in the bottom right plot assume the statistical error for ND280 measurements are much smaller than those of the WAGASCI experiment.

393 **3.3 Extraction of Cross sections**

The flux-integrated CC inclusive cross sections on H₂O and CH are calculated from the number of selected events with background subtraction and efficiency correction

$$\sigma_{CC} = \frac{N_{sel} - N_{BG}}{\phi T \epsilon},$$

394 where N_{sel} is the number of selected events from the real data, N_{BG} is the number of
395 contaminated background events, ϕ is the integrated ν_μ flux, T is the number of target
396 nucleons, and ϵ is the detection efficiency for signal estimated by MC simulation. The
397 number of main background events is effectively estimated from side-band samples. The
398 CH interaction background for the H₂O measurement is estimated from the measurement
399 of the Water-out WAGASCI module and/or the proton module. The neutrino interaction
400 background for the antineutrino measurement is estimated from the opposite-sign inter-
401 actions selected by Baby MIND. The dominant error for the inclusive total cross section
402 measurement is the uncertainty of the neutrino flux, which is $\sim 9\%$ now and is expected
403 to be reduced to $\sim 6\%$. Since the flux error is dominated by the normalization type error,
404 the flux error can be significantly reduced for the relative comparison of the H₂O and CH
405 cross sections and the relative comparison of the ND280 and WAGASCI measurements.
406 For example, T2K INGRID succeeded to determine the cross section ratio for CH and
407 Fe with 3% precision[5]. For the exclusive and/or differential corss section measurements,
408 statistical error would be dominant, size of which depending on the binning.

409 **3.4 Subjects WAGASCI can contribute**

410 Recent accelerator neutrino experiments use nuclear target e.g. organic scintillator, water
411 and iron. So the interaction is largely affected by nuclear effects such as Fermi motion,
412 correlated pairs of nucleons in nucleus (two particles-two holes, 2p2h), collective nuclear
413 effects and final state interactions (FSI) of secondary particles in the nuclei after the initial
414 neutrino interactions.

415 The main interaction type at the T2K energy (sub GeV) is the CC quasi-elastic (CCQE)
416 interaction with nucleons inside nucleus. The energy is reconstructed from the lepton
417 momentum assuming CCQE kinematics in T2K and other interactions would bias the
418 reconstructed energy. Figure 18 shows how the reconstructed energy is affected. The 2p2h
419 interactions mainly happen through the interaction with a correlated nucleons pair and also
420 through the Δ resonance interaction followed by pion-less decay. The 2p2h interactions
421 are observed in electron scattering experiments [8] where the 2p2h events were observed
422 in the gap between quasi-elastic region and pion-production region. Neutrino experiments
423 have attempted to measure the 2p2h interactions, but so far there are only indicative
424 results because the energy spectrum of the neutrino beam is wide and the precision of the
425 event-by-event determination of the neutrino energy is not good nor suffered from bias. Our
426 measurements, when combined with ND280 measurement, will give the cross section values

for narrow energy-spread fluxes and give insight for such interactions. Another efficient way to investigate the 2p2h interaction is direct measurement of proton tracks with low momentum threshold and wide acceptance. Figure 19 left plot shows proton multiplicities for the CCQE events and 2p2h events. Figure 19 right plot shows opening angles of two proton-tracks for the events having two protons. The water-out WAGASCI can provide good sample for the 2p2h interaction search because its low density medium enables the detection of low momentum protons in side acceptance.

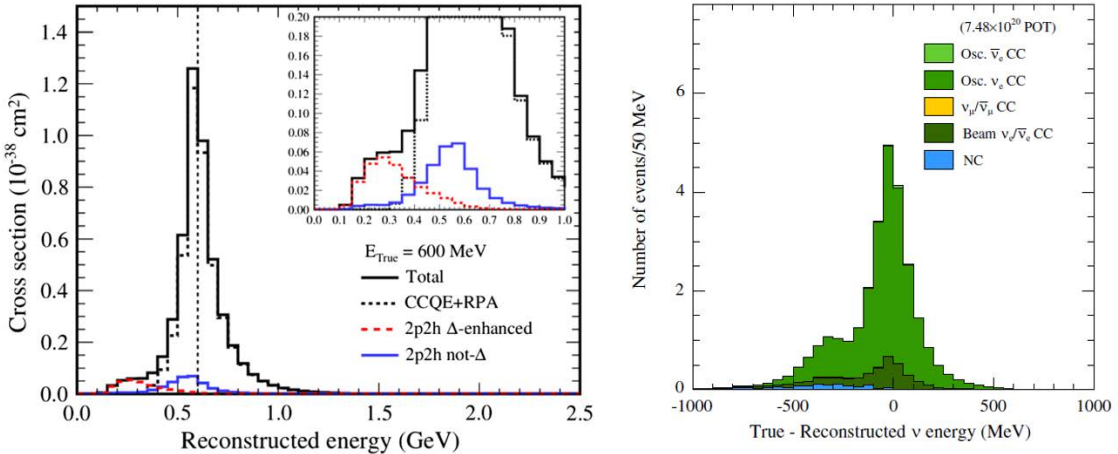


Figure 18: Left: reconstructed neutrino energy for CCQE and 2p2h interactions of 600 MeV muon neutrinos on ^{12}C simulated with a mode. Right: difference between true and reconstructed energy of the ν_e CCQE-like sample. The energy is reconstructed from the lepton momentum assuming the kinematics of the CCQE interaction. Both plots from [2]

There are various models which describe the collective nuclear effects [9]. The wide acceptance of the WAGASCI experiment will provide information complementary to ND280 and will play important role to select and tune models.

T2K is starting to use ν_e CC1 π samples at the far detector to increase the statistics. One of the biggest uncertainty of the CC1 π sample comes from the final state interactions of pions in the nuclei after the initial neutrino interactions because they change the multiplicity, charge and kinematics of the pions. The multi-pion production events can be migrated into the CC1 π sample due to the FSIs, and they become backgrounds. The WAGASCI module has a capability to distinguish the pion track and proton track from dE/dx , so WAGASCI can provide the CC1 π cross section with low momentum threshold and wide acceptance for pion tracks.

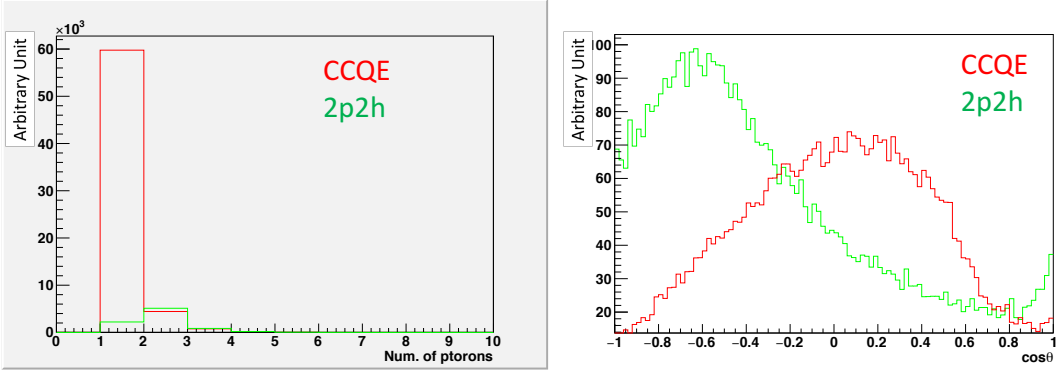


Figure 19: Proton multiplicities (left) and opening angles between two proton tracks (right) for CCQE events and 2p2h events. The final-state interaction is taking into account.

4 Status of J-PARC T59 experiment

We had submitted a proposal of a test experiment to J-PARC in April 2014 to test a new detector with a water target, WAGASCI, at the neutrino monitor hall, and the proposal was approved as J-PARC T59. The project contains the side and downstream muon range detectors as well.

The first WAGASCI module has been constructed in 2016 and installed at the on-axis position in front of the T2K INGRID detector for the commissioning and the first cross section measurement as a part of the T2K experiment. The INGRID electronics boards are used to read the signal. The light yield measured with muons produced by the interaction of neutrinos in the hall wall, shown in Figure 20, is sufficiently high to get a good hit efficiency. A track search algorithm based on the cellular automaton has been developed using the software tools from T2K INGRID. Examples of observed events are shown in Figure 21. The tracking efficiency in a 2-dimensional projected plane was evaluated by comparing the reconstructed track in the WAGASCI module and the INGRID module, and is shown in Figure 22. Note that that the tracking efficiency for high angle (> 70 deg) is not evaluated because of the acceptance of the INGRID module, not because of the limitation of the WAGASCI module.

In 2017 Autumn, the construction of the second WAGASCI module and the dedicated electronics board were completed. The module and the electronics were install on the B2 floor together with the T2K proton module and the INGRID module as shown in Figure 23. The proton module is to be used as the entering muon veto and also for the comparison of interaction between CH and Water. The INGRID module will act as the muon detector for this period but due to its limited acceptance angle this is only a temporary measure.

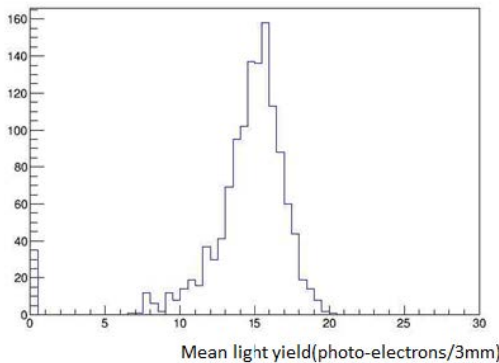


Figure 20: Light yield for muons produced by the interaction of neutrinos in the hall wall. Average light yields for each channel are plotted.

468 The detector was commissioned and since October has been in operation taking data with
469 the T2K antineutrino beam.

470 The production of the components of the side muon range detectors has been completed
471 and now the detectors are being assembled at the Yokohama National University. These
472 detectors will be installed between January and June 2018, when T2K is not running.

473 The Baby MIND detector was transported from CERN to Japan in December, 2017.
474 It will be installed and commissioned in Jan.-Feb. 2018 and T59 will take the neutrino-
475 induced muon data in April and May.

476 5 MC studies

477 5.1 Simulation setup

478 The expected number of neutrino events in the water-in Wagasci detector is predicted by
479 Monte Carlo simulations. Neutrino beam flux at the detector location is simulated by
480 T2K neutrino flux generator, JNUBEAM. Neutrino interactions with target materials are
481 simulated by a neutrino interaction simulator, NEUT. Detector responses are simulated
482 using GEANT4-based simulation.

483 The detector geometry in the simulation so far is different from the actual setup as
484 shown in Figure 24. The active neutrino target region consists of four WAGASCI modules.
485 The size of the WAGASCI module is same as the actual one: 1000 mm × 1000 mm in the
486 x and y directions and 500 mm along the beam direction (z-direction). Two Side-MRD
487 modules are installed either side of the Wagasci modules. Each Side-MRD module consists
488 of ten iron plates whose dimension is 30 mm (thickness) × 2000 mm (height) × 3200 mm

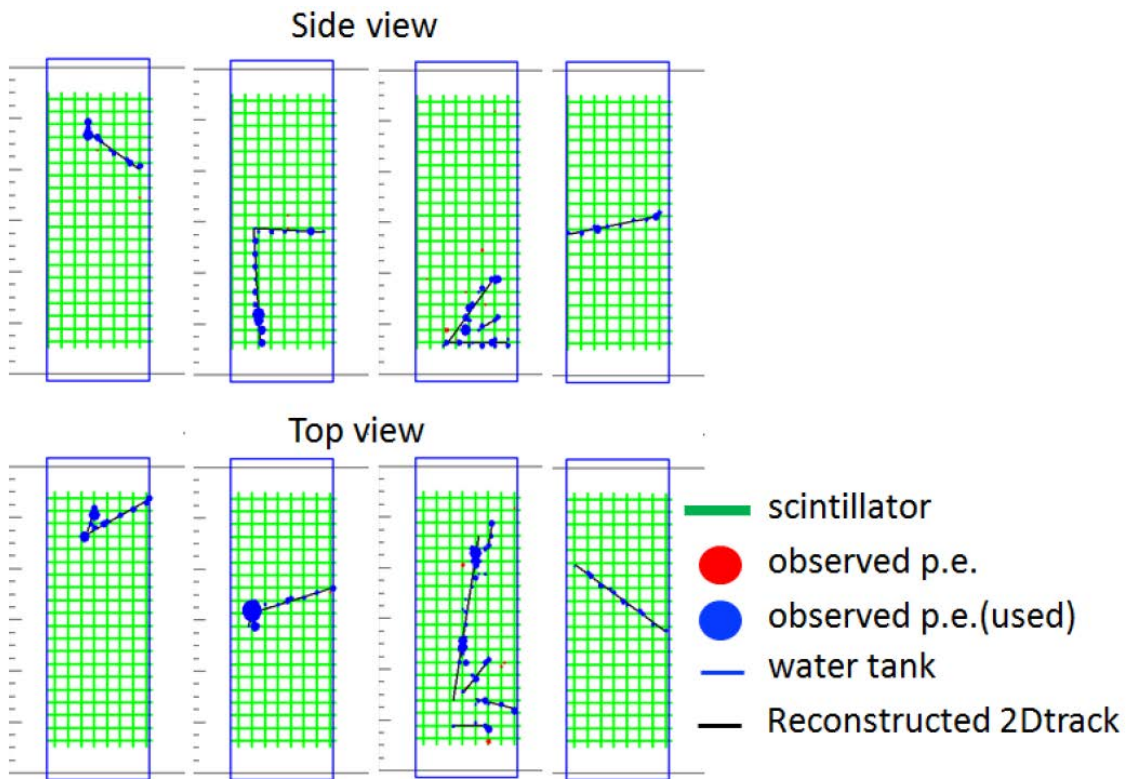


Figure 21: Example event displays of the WAGASCI module at on-axis. The reconstructed tracks are overlaid.

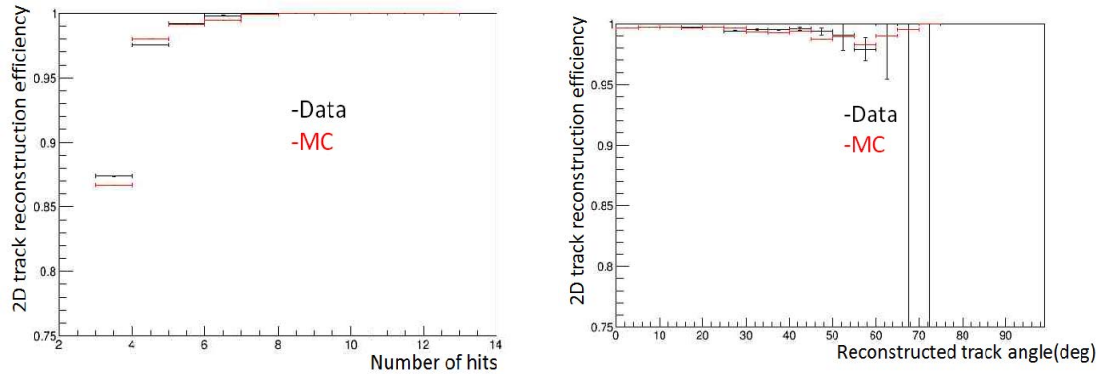


Figure 22: 2D track reconstruction efficiency as a function of number of hits (left) and track angle (right). Here the track angle is the one reconstructed by the INGRID module.

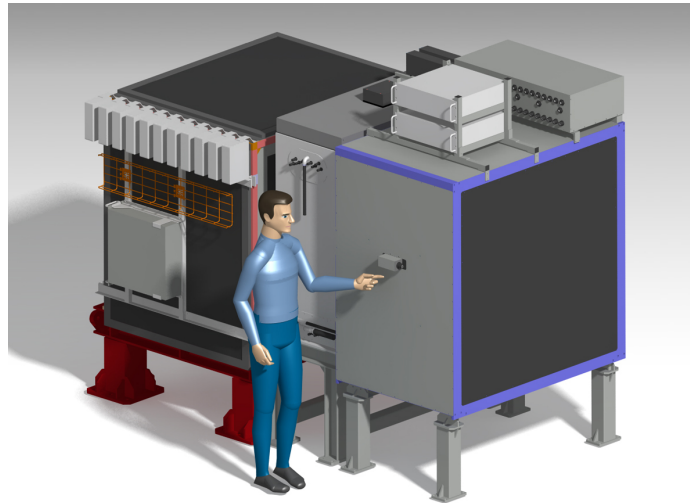


Figure 23: J-PARC T59 detector configuration in October 2017.

489 (width). The distance between the Side-MRD modules and WAGASCI modules is 800
 490 mm. The downstream-MRD is equivalent to the Baby-MIND, but without the magnetic
 491 field. It consists of thirty iron plates whose dimension is 30 mm (thickness) \times 2000 mm
 492 (height) \times 4000 mm (width). The distance between the downstream-MRD modules and
 493 WAGASCI modules is 800 mm. Update of the study with the actual geometry is now
 494 underway.

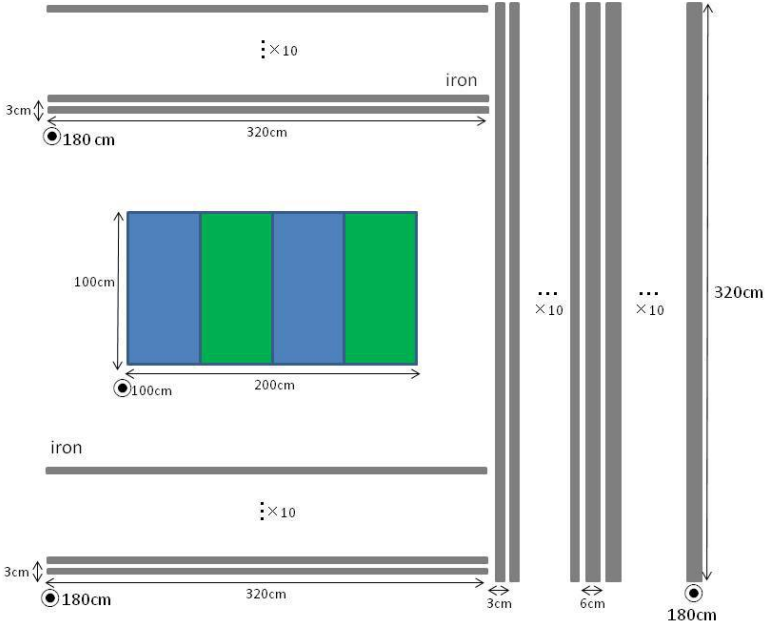


Figure 24: Geometry of the detectors in the Monte Carlo simulation.

495 To simulate the signal, the energy deposit inside the scintillator is converted into the
 496 number of photons. The effects of collection and attenuation of the light in the scintillator
 497 and the WLS fiber are simulated, and the MPPC response is also taken into account. The
 498 light yield is smeared according to statistical fluctuations and electrical noise.

499 5.2 Event selection

500 Tracks are reconstructed in two-dimensional planes in each sub-detector. Then, track
 501 matching among the sub-detectors and three-dimensional track reconstruction are per-
 502 formed. These analysis tools have been developed from the software tools by the T2K
 503 INGRID and in mature stage already.

504 The events are selected as follows. The starting point of the track is required to be

505 50 mm away from the edge of the WAGASCI module. This is to remove the background
 506 from the outside. The longest track has to penetrate more than one (five) iron plates in
 507 Side-MRD modules (Baby-MIND). This cut select a muon track and rejects backgrounds
 508 from NC and neutral particles. Then, in order to determine the muon momentum, it is
 509 required that the longest track stops in MRDs (Side-MRD modules and Baby-MIND) or
 510 penetrate all iron plates.

511 Table 1 shows numbers of the selected events in one water-in WAGASCI module after
 512 the event selection. We expect 4,239 (1,666) events from charged-current interaction on
 513 H_2O with 5×10^{20} POT in (anti)neutrino-mode with one water-in WAGASCI module.
 514 The purity, when interactions on CH is counted as background, is 78% for the neutrino-
 515 mode. There is a significant contamination from the wrong-sign (neutrino) interaction for
 516 antineutrino-mode, however, we expect that it will be removed with efficiency higher than
 90% by Baby MIND.

Table 1: Expected number of the selected neutrino-candidate events in one water-in WAGASCI module with 5×10^{20} POT in each of neutrino-mode and antineutrino-mode. Note that the wrong sign component will be reduced by one order by applying the charge selection by Baby MIND.

	CC on H_2O	NC on H_2O	Interaction on CH	wrong sign interaction
ν -mode	4239	107	1087	(negligible)
anti- ν -mode	1666	14	560	(561)

517
 518 Table 2 and 3 summarize contributions classified by the interaction types and final state
 topologies for the selected charged current-interaction events, respectively.

Table 2: Interaction types for the selected charged-current events.

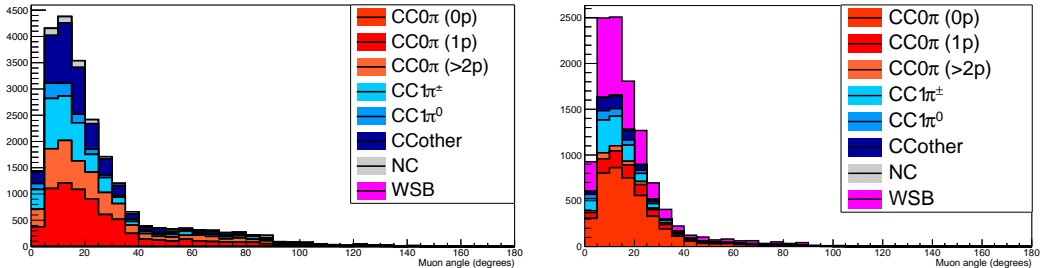
	CCQE	2p2h	CC resonant π	CC-DIS
ν -mode	48.4 %	9.7 %	27.1 %	14.7 %
anti- ν -mode	57.1 %	8.2 %	17.3 %	17.3 %

Table 3: Final state topologies for the selected charged-current events.

	CC0 π	CC1 π	CC2 π	CCn π
ν -mode	67.4 %	20.9 %	3.0 %	8.7 %
anti- ν -mode	79.5 %	16.3 %	1.2 %	3.0 %

519

520 Figure 25 shows the reconstructed angles of the longest tracks in the selected events in
 521 the neutrino-mode and the anti-neutrino mode. Figure ?? shows the iron plane numbers
 522 in Side-MRD and Baby-MIND corresponding to the end points of the longest tracks in the
 selected events in the neutrino-mode and the anti-neutrino mode.



523 Figure 25: The reconstructed angles of the longest tracks in the selected events in the
 neutrino-mode (left) and the antineutrino-mode (right).

524

6 Standalone WAGASCI-module performances

525 In the previous sections, the WAGASCI detector was studied using the Muon Range Detectors.
 526 In this section, the standalone abilities of WAGASCI module are presented. Using
 527 the WAGASCI configuration presented in Section 5, we have evaluated that only 7% of
 528 the muons will be stopped in one of the WAGASCI modules. However, this proportion
 529 increases to 53% for pions and 73% for protons produced by neutrino interactions at 1.5°
 530 off-axis. Figure 27 shows the momentum distribution of these daughter particles as well as
 531 for the sub-sample stopped in one of the WAGASCI modules. Therefore, the study of the
 532 standalone abilities of the WAGASCI module in this section are dominantly motivated by:

- 533 • the accurate measurement of the neutrino interaction final states. Though most of
 534 the muons will be reconstructed and identified in the MRDs, the hadronic particles
 535 will predominantly stop in one of the WAGASCI modules. One has therefore to rely
 536 exclusively on the WAGASCI module information alone to reconstruct, identify and
 537 measure the momentum of pions or protons.
- 538 • the coverage of the MRDs is not 4π . Using the WAGASCI module information can
 539 therefore help to constrain the particles that exit the WAGASCI module but do not
 540 enter any MRD.
- 541 • the particle identification of low momenta muons $p_\mu < 300$ MeV/c that will leave
 542 only a few hits in the MRD. Using the WAGASCI module information will clearly
 543 enhance the particle identification.

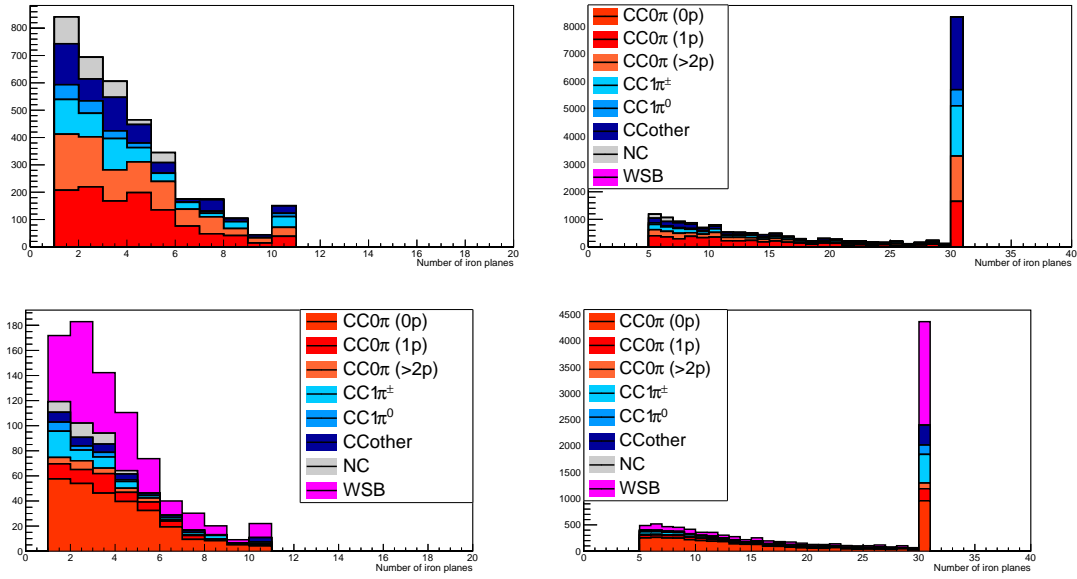


Figure 26: Iron plane numbers in Side-MRD (left) and Baby-MIND (right) corresponding to the end points of the longest tracks in the selected events in the neutrino-mode (top) and the antineutrino-mode (bottom).

544 This study is based on an original study done for the ND280 upgrade target, with some
 545 modifications. Though the cell size is similar to the WAGASCI configuration presented
 546 in Section 5, the external dimensions are different (1864 mm \times 600 mm \times 1300 mm).
 547 Whenever the results are presented with this external size and this parameter is likely to
 548 impact the result, it will be mentioned.

549 Note that in this section, a simplified reconstruction algorithm presented in Section 6.1 is
 550 used. The fiducial volume is chosen accordingly as the inner cube of the module which
 551 surfaces are $4 \times$ scintillator space = 100 mm distant from the module external surfaces.
 552 The neutrino interactions are simulated using NEUT v5.3.2. The NEUT input neutrino
 553 flux is estimated using JnuBeam v13a and assuming the detector to be located at 1.5°
 554 off-axis, as in Section 5. Note that the event reconstruction efficiency as a function of true
 555 neutrino energy might be changed at 1.5° , due for example to different Q^2 distributions.
 556 For this reason, one has to note that the reconstruction results might change slightly from
 557 2.5° and 1.5° . To avoid a similar change on the particle-only reconstruction efficiencies,
 558 they will be presented as a function of variables that completely characterize the particle
 559 kinematic state, *i.e.* its momentum and angle. Figure 28 shows the vertex distributions
 560 of the daughter particles of neutrinos interacting one standard WAGASCI water-module.
 561 In this section, we will show the detector reconstruction and particle identification in this

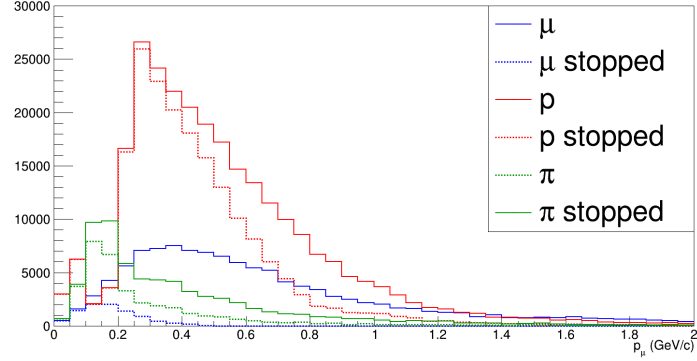


Figure 27: Momentum distribution of true particles in WAGASCI (plain) and corresponding distributions only for particles stopping into the WAGASCI module (dashed).

562 phase space, both for leptonic and hadronic particles. We will finally show an empty
 563 WAGASCI module can highly enhance the ability to constrain the neutrino interaction
 564 final state which is critical to reduce the corresponding uncertainties.

565 6.1 Reconstruction algorithm

566 6.1.1 Description

567 For this section, an ideal “simulated” reconstruction is developed. A particle is recon-
 568 structed if:

- 569 1. The particle is charged.
 570 2. Has at least one hit (energy deposit > 2.5 photo-electron) in a scintillator.
 571
- 572 3. The particle enters one TCP and has one hit in the tracker.
 573 Or

- 574
- 575 • The particle should be long enough to be reconstructed by the detector in at
 576 least 2 out of 3 views (XZ, YZ, XY). The length criterion requires the particle
 577 to let at least 4 hits in the detector. In the “less favourable case” of pure
 578 longitudinal or transverse going tracks, it represents a the track length of $L_{track} \geq$
 579 $4 \times$ scintillator space = 100 mm.
 - 580 • In the views where particles pass the length criterion, the particle shall not
 581 be superimposed with longer tracks in at least two views. The superposition
 582 criterion is estimated with the distance inter-tracks (DIT) which corresponds to

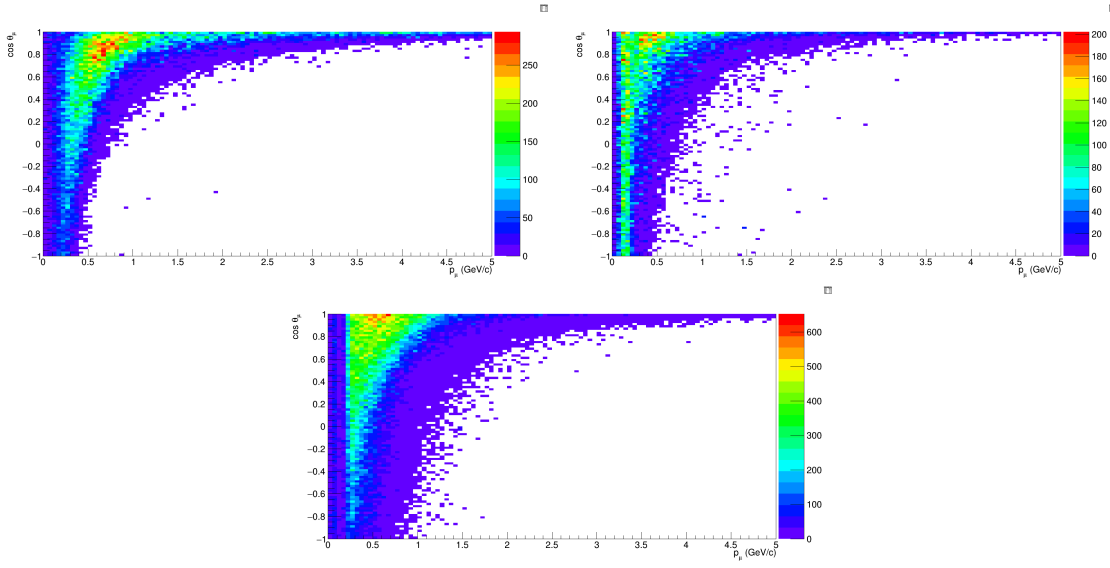


Figure 28: True number of muons (left), charged pions (right) and protons (bottom) in the two WAGASCI water-module as a function of the particles momenta and angles at 1.5° .

583 the orthogonal distance between two tracks at the ending point of the shortest
 584 distance (see Figure 29). For a track we call track 1, the super position criterion is
 585 tested with every longer track that starts at the same vertex. Let \vec{p}_1 the vector
 586 of track 1, and p_1^a its projections in the XZ, YZ and XY planes respectively for
 587 *i*=1,2,3. Note that these are projections onto 2D planes and not onto a direction
 588 vector. this case, the relative angle between track 1 and a longer track, track 2,
 589 (of vector \vec{p}_2) in a view a is given by:

$$\cos \theta = \frac{\vec{p}_1^a \cdot \vec{p}_2^a}{\|\vec{p}_1^a\| \|\vec{p}_2^a\|} \quad (1)$$

590 and the distance inter track is given by:

$$DIT = \|\vec{p}_1^a\| \sin \theta \quad (2)$$

591 The DIT should be higher than $4 \times$ scintillator width for the track 1 to be not
 592 superimposed with the track 2 in the view a, which also corresponds to 100 mm
 593 in the nominal configuration.

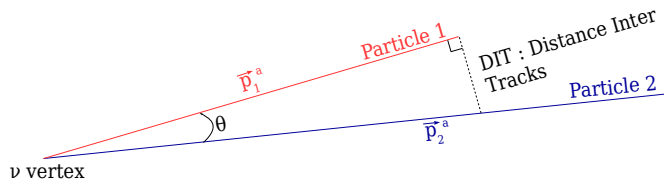


Figure 29: Definition of the distance inter tracks.

594 6.1.2 Performances

595 The particle-only reconstruction efficiencies and the reconstruction threshold in momenta
 596 are shown in Table 4. This threshold is defined as the maximal momentum for which the
 597 reconstruction efficiency is smaller than 30%. The thresholds in muon and pion momenta
 598 are 150 MeV/c. Most of the muons are above this threshold (see Figure 28) which leads
 599 to a 79% reconstruction efficiency.

	μ	π	p
Reconstruction Efficiency	79%	52%	26%
Momentum threshold	150 MeV/c	150 MeV/c	550 MeV/c

Table 4: Reconstruction efficiency and momentum threshold for muons, pions and protons. The threshold is defined as the maximal momentum for which particles have a reconstruction efficiency smaller than 30%.

600 The lower pion and proton efficiencies (respectively 52% and 26%) are due to lower
 601 efficiencies for similar momenta than muons, coming from strong interactions as shown
 602 on Figures 30. Efficiencies of each particle type tend to decrease in the backward region
 603 due to lower particle momenta. However, for a fixed momentum value, the reconstruc-
 604 tion efficiency is almost uniform which confirms the ability of the WAGASCI detector to
 605 reconstruct high angle tracks.

606 The reconstruction is thereafter tested on neutrino events. Table 5 summarizes the
 607 number of reconstructed events and efficiencies for each interaction type. As expected
 608 from the high muon reconstruction efficiency, the charged current interactions have recon-
 609 struction efficiencies $\geq 85\%$.

610 The reconstruction efficiencies as a function of the neutrino energy and muon kinematics
 611 are respectively shown on Figure 31 and 32.

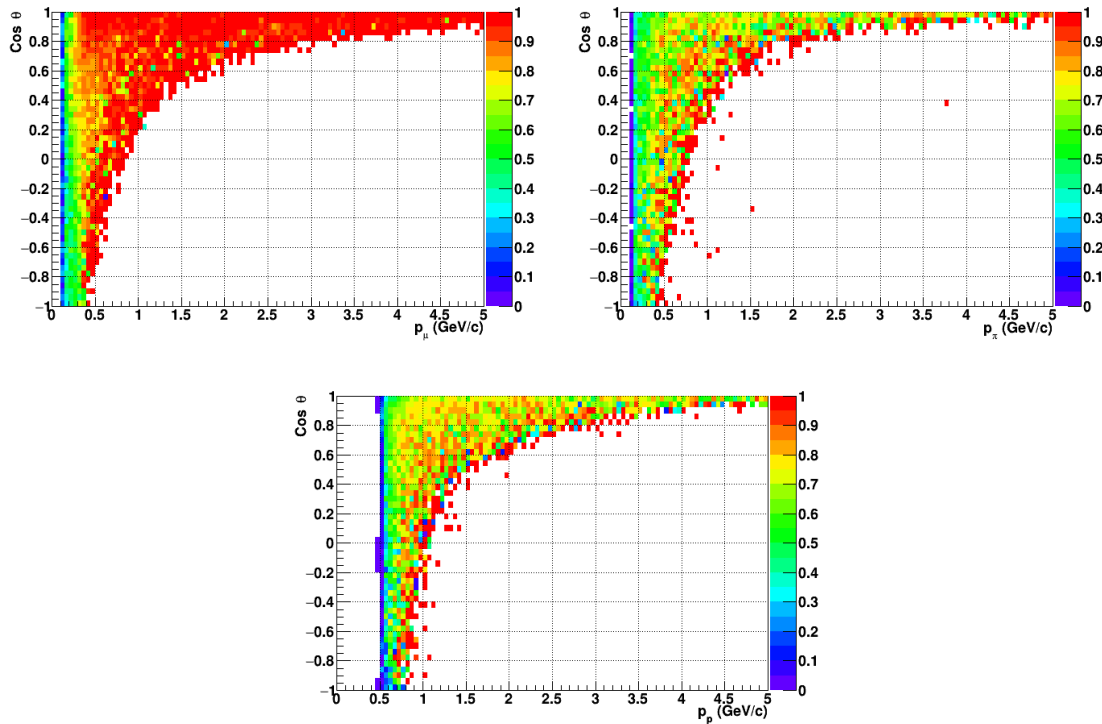


Figure 30: Reconstruction efficiency of muons (left), charged pions (right) and protons (bottom) in the WAGASCI water-module as a function of the particles momenta and angles.

	CC0 π	CC1 π	CCOthers	NC	All
Reconstruction efficiency	85%	87%	91%	22%	68%

Table 5: Number of true interactions reconstructed. The purity and reconstruction efficiency of each true interaction is also shown.

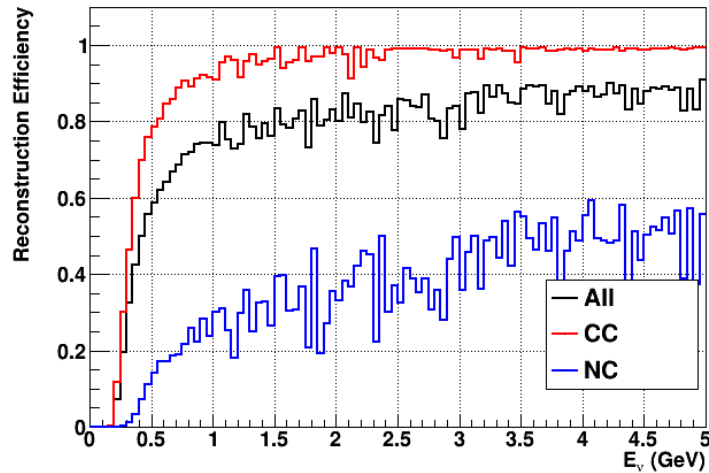


Figure 31: Reconstruction efficiency of all neutrino (black), CC (red) and NC (blue) interactions in the WAGASCI water-module as a function of the neutrino energy.

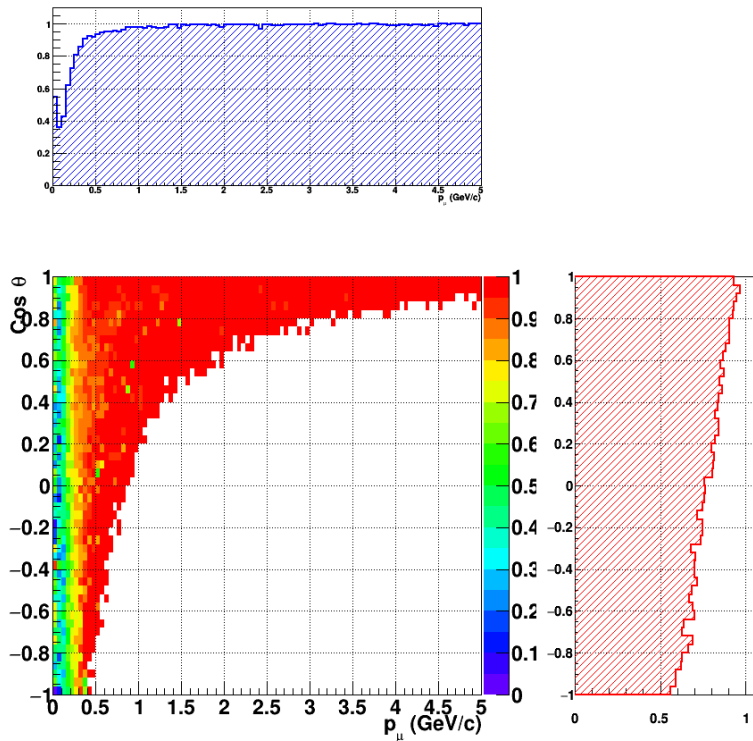


Figure 32: Reconstruction efficiency of CC interactions in the WAGASCI water-module as a function of the muon kinematic variables (momentum and angle).

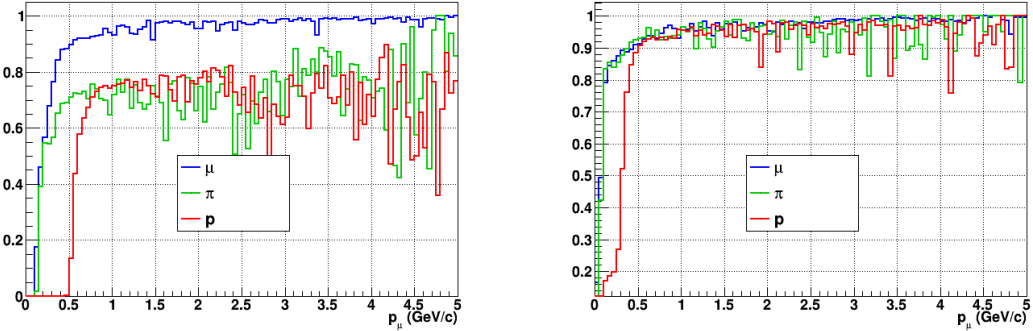


Figure 33: Reconstruction efficiency for muons, pions and protons in the water-in (left) and water-out (right) modules.

Note that a Particle Identification Algorithm has been also developed. It is based on the charge deposition of the particles in the scintillator, of the detection of a decay-electron. However, information depends highly on the number of scintillator hits by a particle, which creates an important difference between a real WAGASCI module and the one used for the ND280-upgrade simulation. For this reason, the corresponding results will not be detailed here, but can be found in [?].

6.2 Background subtraction: the water-out module

In the nominal configuration, 20% of the neutrino interactions occurs on scintillators (C_8H_8). This background should be removed in order to measure the neutrino interaction on the same target as Super-K, which suppress the differences in cross-section models. For this purpose, we propose to use a water-out module, where the water is replaced by air. The detector is therefore fully active and has a 3 mm spatial resolution (scintillator thickness) which create an ideal detector to reconstruct and identify hadrons, and study np-nh interactions. The counter-part is the difference in particle energy deposition between the water and this water-out module that will need to be corrected for. In this section, we present the capabilities of such a module, and the impact it can have on cross-section measurements for the neutrino community in general and T2K in particular. The same reconstruction and selection as the water-in module is applied. Figure 33 shows the comparison between the water-in and the water-out reconstruction efficiencies for muon, pions and protons. 90% of the muons and 87% of the pions are reconstructed, while 70% of the protons are even reconstructed. It allows to lower down the proton threshold to 250 MeV/c (see Table 6).

As a consequence of tracking even low momenta particle, the reconstruction efficiency is uniform and almost maximal on the entire $\cos \theta_\mu$ phase space, as shown on Figure 34.

	μ	π	p
Reconstruction Efficiency Momentum threshold	90% 50 MeV/c	87% 50 MeV/c	70% 250 MeV/c

Table 6: Reconstruction efficiency, proportions of μ -like and non μ -like and momentum threshold for muons, pions and protons in the empty module. The threshold is defined as the maximal momentum for which particles have a reconstruction efficiency smaller than 20%.

636 Since the fiducial mass represents 0.25 tons, the total number of events is divided by a
 637 factor of 3 compared to the water-in module. The water-out module offers interesting
 638 possibilities to study np-nh interaction since 70% of the protons are reconstructed. In the
 639 future, a possible separation as a function of the number of proton track will be studied.
 640 Moreover, we are currently pursuing the use of single and double transverse variables (cite
 641 Xianguo) to open new possibilities for separating np-nh from Final State Interactions, or
 642 for isolating the interactions on hydrogen from interactions on carbon in this module.

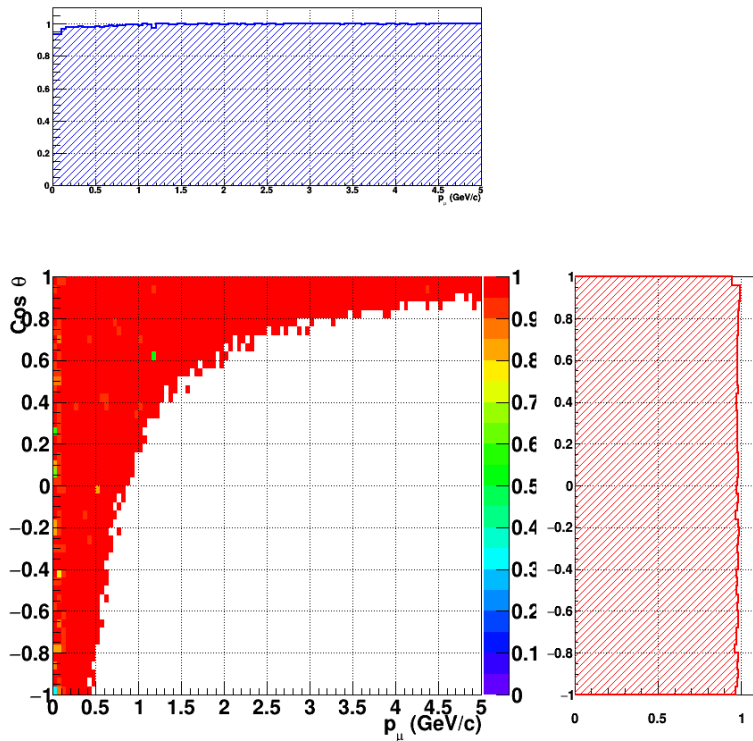


Figure 34: Reconstruction efficiency of CC interactions in the WAGASCI empty module as a function of the muon kinematic variables (momentum and angle).

643 **7 Schedule**

644 We would like to start a physics data taking from T2K beam time after the summer
645 shutdown in 2018. By then, commissioning and tests of the detectors will be completed
646 in J-PARC T59. The experiment can run parasitically with T2K, therefore we request no
647 dedicated beam time nor beam condition as discussed in the following section.

648 Once the approved POT is accumulated, the WAGASCI modules will be removed
649 from the experimental site, but we would like to keep the Baby-MIND and the Side-MRD
650 modules on the B2 floor of the NM pit as common platforms of future neutrino experiments
651 using the T2K neutrino beam.

652 **8 Requests**

653 **8.1 Neutrino beam**

654 The experiment can run parasitically with T2K, therefore we request no dedicated beam
655 time nor beam condition. As data taking periods, we request the ‘nominal’ T2K one-year
656 operation both for the neutrino beam and the antineutrino beam. The T2K has been
657 requesting 0.9×10^{21} POT/year and actually accumulating about 0.7×10^{21} POT/year in
658 recent years. For each year, starting from the Autumn, T2K is running predominantly in
659 the neutrino mode or in the antineutrino mode. Our request is to have one-year neutrino-
660 mode data and another one-year antineutrino mode data assuming that the POT for the
661 fast extraction in each year is more than 0.5×10^{21} POT.

662 **8.2 Equipment request including power line**

663 We request the followings in terms of equipment on the B2 floor:

- 664 • Site for the WAGASCI modules, Side-MRD modules and BabyMIND and their elec-
665 tronics system on the B2 floor of the near detector hall (Figure 2 and 3).
- 666 • Anchor points (holes) on the B2 floor to secure the WAGASCI modules, Side-MRD
667 module and Baby-MIND, detailed floor plans to be communicated in a separate
668 document.
- 669 • Power line for the magnets in Baby-MIND: 400 V tri-phase 48-to-62 Hz, capable of
670 delivering 12 kW. We have a wish for the magnet power line to be installed and
671 available to us by beginning of March 2018.
- 672 • Electricity for electronics and water circulation system, 3 kW, standard Japanese
673 electrical sockets.

- 674 1. Online PCs: 2.1 kW

675 2. Electronics: 0.7 kW

676 3. Water sensors: 1 kW

- 677 • Air conditioner for cooling heat generation at Baby-MIND magnets, online PCs and
678 electeronics
- 679 • Beam timing signal and spill information
- 680 • Network connection

681 The infrastructure for much of the above exists already. Exceptions are the power line
682 for the magnet and the electronics and holes in the B2 floor to anchor the detector support
683 structures.

684 References

- 685 [1] K. Abe et al. Measurement of the muon neutrino inclusive charged-current cross
686 section in the energy range of 13 GeV with the T2K INGRID detector. *Phys. Rev.*,
687 D93(7):072002, 2016.
- 688 [2] K. Abe et al. Measurement of neutrino and antineutrino oscillations by the T2K
689 experiment including a new additional sample of ν_e interactions at the far detector.
690 *Phys. Rev.*, D96(9):092006, 2017.
- 691 [3] M. Antonova et al. Baby MIND Experiment Construction Status. In *Prospects in*
692 *Neutrino Physics (NuPhys2016) London, London, United Kingdom, December 12-14,*
693 2016, 2017.
- 694 [4] K. Nitta et al. The k2k scibar detector. *Nucl. Instrum. Meth. A*, 535:147, 2004.
- 695 [5] K. Abe et al. (T2K Collaboration). Measurement of the inclusive ν_μ charged current
696 cross section on iron and hydrocarbon in the t2k on-axis neutrino beam. *Phys. Rev.*
697 D, 90:052010, 2014.
- 698 [6] F. Magniette F. Gastaldi, R. Cornat and V. Boudry. A scalable gigabit data acquisition
699 system for calorimeters for linear collider. *proceedings of TIPP2014*, page PoS 193,
700 2014.
- 701 [7] J. Fleury, S. Callier, C. de La Taille, N. Seguin, D. Thienpont, F. Dulucq, S. Ahmad,
702 and G. Martin. Petiroc and Citiroc: front-end ASICs for SiPM read-out and ToF
703 applications. *JINST*, 9:C01049, 2014.
- 704 [8] M. B. Barbaro J. A. Caballero T. W. Donnelly G. D. Megias, J. E. Amaro. Inclusive
705 electron scattering within the susav2 meson-exchange current approach. *Phys. Rev.*
706 D, 94:013012, 2016.

- 707 [9] M. Valverde J. Nieves, J. E. Amaro. Inclusive quasi-elastic neutrino reactions. *Phys.*
708 *Rev. C*, 70:055503, 2004.
- 709 [10] Yu. G. Kudenko, L. S. Littenberg, V. A. Mayatsky, O. V. Mineev, and N. V. Ershov.
710 Extruded plastic counters with WLS fiber readout. *Nucl. Instrum. Meth.*, A469:340–
711 346, 2001.
- 712 [11] O. Mineev, Yu. Kudenko, Yu. Musienko, I. Polyansky, and N. Yershov. Scintillator
713 detectors with long WLS fibers and multi-pixel photodiodes. *JINST*, 6:P12004, 2011.
- 714 [12] Etam Noah et al. Readout scheme for the Baby-MIND detector. *PoS*, Pho-
715 toDet2015:031, 2016.
- 716 [13] Omega. Spiroc 2 user guide. 2009.